ORIGINAL ARTICLE

Highly Stable Plasmonic Nanostructures on a Nickel-Sputtered Glass and Polymeric Optical Fiber Sensors

Hariharan Manoharan[1] · Dharanibalaji KC[2] · V. V. R. Sai[1]

Abstract

This study shows development of highly sensitive and stable localized surface plasmon resonance (LSPR)-active U-bent glass and polymeric optical fiber (GOF and POF) sensor probes by a seed-mediated in situ growth technique. Here, the nickel/nickel oxide seeds (Ni/NiO, 3 to 5 nm size) were formed on the U-region of the fiber probe by sputter coating nickel under a low vacuum (3 Pa), and then, gold nanostructures (AuNSs) were grown over the Ni/NiO seeds. The evanescent wave absorbance (EWA) phenomenon in the U-bent fiber probe was exploited to monitor the growth kinetics of AuNSs in real-time. Experimental observations point to a potential galvanic replacement of Ni by Au. The newly formed AuNSs on U-bent GOF and POF probes gave rise to a LSPR-based refractive index sensitivity of 27.66 and 25.65 $\Delta A/\Delta RIU$ with plasmonic peak at 600 and 570 nm, respectively. These plasmonic probes show an excellent chemical and mechanical stability, in addition to high surface enhanced Raman scattering (SERS) activity. This quick and facile technique is highly suitable for large-scale manufacture of reliable plasmonic fiber optic sensor probes for chemical and bio sensing applications.

Keywords U-bent glass and polymeric optical fiber · Plasmonic sensors · Evanescent wave absorbance · Ni sputtered seeds · Seed-mediated growth · Stable gold nanostructures

Introduction

Over the past two decades, plasmonic fiber optic sensors have emerged as an important tool to detect ultra-low concentrations of analytes such as proteins, DNA, biomarkers, toxins, pathogens, as well as toxic vapors [1–3]. Plasmonic fiber optic sensors typically employ either continuous or discrete noble metal nanostructures for sensing that rely on the surface plasmon resonance (SPR) or localized surface plasmon resonance (LSPR) phenomena, respectively [4, 5]. In particular, LSPR sensing techniques provide high refractive index (RI) sensitivity and high-end device miniaturization with multiplexing capabilities [6, 7]. The fiber optic sensor probe (transducer) allows an efficient excitation of the fiber core surface-bound noble metal nanostructures by the evanescent field at the fiber core-medium interface and real-time monitoring of their LSPR spectral characteristics. By the virtue of LSPR phenomenon, the characteristic optical absorption spectrum of the noble metal nanostructures depends on their shape, size, inter-particle spacing and the dielectric properties of the surrounding medium. In a plasmonic fiber optic sensor, nanostructures contribute to the improvement in sensitivity, selectivity, and detection limits [8].

Glass (fused silica) and polymeric (or plastic, mainly polymethylmethacrylate—PMMA) optical fiber (GOF and POF, respectively) probes have been the most widely utilized optical waveguides in evanescence wave absorbance (EWA)-based plasmonic fiber optic sensors for sensing biochemicals, gases, explosives, and heavy metals [9–11]. The fiber core region decorated with metallic nanostructures has also been employed for measuring temperature, pH, refractive index, salinity, humidity, and micro-displacement [12–16]. While gold as well as silver nanostructures have been routinely used for plasmonic sensor [17], gold nanostructures (AuNSs) are the preferred choice due to their chemical inertness and have established facile synthesis and functionalization protocols [18]. In addition, robustness of the nanostructures and a rugged sensor design to withstand and tolerate harsh environmental conditions are also important for the practical applications [19].

✉ V. V. R. Sai
vvrsai@iitm.ac.in

[1] Biomedical Engineering Laboratory, Department of Applied Mechanics, Indian Institute of Technology Madras, Chennai 600036, India

[2] Department of Chemical Engineering, Indian Institute of Technology Madras, Chennai 600036, India

The conventional techniques for the fabrication of plasmonic fiber optic sensor probes involve either sputtering of gold [20, 21] over a decladded fiber or chemisorption of gold nanostructures to thiol or amine-functionalized fiber core surface [22]. Both of these techniques have their own advantages and limitations. For example, sputter coating of gold or silver or any other lesser known plasmonic materials such as copper is an easily scalable fabrication process, however, with a limited control over the size and shape of the nanostructures. Additionally, a thin buffer layer of Cr, Ti, or Ni is pre-coated on the fiber probe surface, mainly to improve the adhesion [23, 24]. This buffer layer impedes the optical properties of the newly sputtered gold films [25]. Further, sputtering technique has been extensively used for fabricating SPR rather than LSPR sensors. On the other hand, the self-assembly of chemically synthesized AuNSs on fiber probe surface mediated by chemisorption and electrostatic interactions allows freedom to utilize the AuNSs of desired size, shape, and thus LSPR spectral characteristics can be precisely controlled by the solution-phase synthesis. However, the stability of the such nanostructured layers is poor and multilayer formation and particle aggregation cannot be ruled out [26, 27]. Therefore, a combination of physical sputter deposition for seed formation and a chemical synthesis route for AuNSs growth is anticipated to be a favorable approach to achieve a robust and highly sensitive plasmonic-LSPR sensors. A seed-mediated growth-based fabrication of plasmonic fiber optic sensors, demonstrated elsewhere by our group [28], could be a highly suitable strategy to explore the combination of physico-chemical process for this purpose.

Ni/NiO nanostructures are known for their excellent electrical and optical properties with high durability and affinity towards dielectric surface [29–31]. Sputtered Ni/NiO films have been widely used in the fabrication of solar cells, photoanodes in water oxidation, and gas sensors [32–34]. In our approach, the Ni/NiO-sputtered seed layer on the U-bent GOF and POF probes was used as a sacrificial template for gold nanostructure (AuNSs) synthesis mediated by galvanic replacement [35]. The seed layer and the AuNSs on the fiber probe were characterized by atomic force and electron microscopic techniques. The LSPR activity and sensor performance of the newly fabricated plasmonic fiber probes were evaluated based on their refractive index sensitivity. Additionally, their chemical and mechanical stability was studied by subjecting the probes to highly acidic or basic solution. Further, the surface enhanced Raman scattering (SERS) activity of the plasmonic POF probes was also investigated.

Materials and Methods

Materials

Multimode polymer clad-fused silica optical fibers (FT200UMT) and fluoropolymer clad polymethylmethacrylate (PMMA) optical fibers (Super ESKA SK10) were procured from Thorlabs Inc., USA and Mitsubishi Chemical Corporation, Japan, respectively. The core diameter, cladding thickness, and numerical aperture of the GOF and POF were 200 μm, 15 μm, 0.39 and 240 μm, 10 μm, 0.5, respectively. Gold chloride trihydrate ($HAuCl_4 \cdot 3H_2O$, ≥99.9%) from Alfa Aesar, silver nitrate ($AgNO_3$) from Merck, ascorbic acid, and cetyltrimethylammonium bromide (CTAB) from SRL chemicals were used for synthesis. All the chemicals including the organic solvents used for cleaning and buffer preparation were of analytical grade. Deionized water (Millipore water, 18 MΩ cm) was used in the experiments.

Fabrication of U-Bent Optical Fiber Probes

U-bent GOF probe was fabricated by following a procedure as depicted in Fig. S1 (in Supplementary Information) and described elsewhere [36]. Briefly, straight silica fiber of length 30 cm was cut using a fiber scribe and the fiber ends were polished. The buffer and the cladding layers in the middle of fiber over a length of 1 cm were removed (decladding) using a sharp stainless-steel razor. The decladded region of the silica fiber was exposed to a butane flame (at ~700 °C) and manually bent to obtain U-bent probe. Subsequently, the U-region (sensor surface) was washed with acetone, piranha solution (70% sulfuric acid + 30% hydrogen peroxide; caution: piranha solution is highly corrosive), and excess DI water.

The U-bent POF probe was prepared by following a procedure as depicted in Fig. S2 (in Supplementary Information) and described elsewhere [37]. Briefly, a straight PMMA fiber of length 30 cm was cut using a POF cutter tool. The central region of the straight PMMA fiber was folded in the form of U-shape and pushed into a glass capillary tube with 1.2 mm inner diameter. Next, the glass capillary containing the fiber was kept in a hot air oven at 80 °C for 15 min, in order to subject the fibers to a thermal deformation to obtain a U-shape. The probe was taken out from the glass capillary and the U-region was dipped in ethyl acetate (3 min) to remove the cladding. Finally, the U-region was cleaned with fiber wipes and washed with excess deionized (DI) water. Using an optical microscope, bend diameter at the U-region was found to be 1.0 ± 0.2 mm and 1.0 ± 0.3 mm for POF and GOF probes, respectively.

Nickel Sputter Deposition

To obtain the seeds over the U-bent region of the probe, Ni sputtering was carried out using Hitachi E-1010 ion sputter coater unit. Inside the sputtering chamber, U-bent probes were placed vertically on a customized mechanical stage as shown in Fig. 1a. The distance between the tip of U-bent probe and the Nickel target (99% pure, purchased from a local vendor) was maintained at 7 cm. Ni sputtering was carried out for a duration of 10 s at 3 Pa pressure, 25 mA

current, 123 W discharge power. Further, the Ni-sputtered probes were stored in a vacuum desiccator and used within 2 days (Fig. 1c).

Growth Solution and in Situ Synthesis of AuNSs

An aqueous solution consisting of $HAuCl_4$, CTAB (surfactant), and ascorbic acid (reducing agent) was used as the growth solution for synthesizing AuNSs on U-bent probes. The Ni-sputtered U-region of the probe was immersed in a sample holder and thoroughly washed with DI water (Fig. 1b). Subsequently, the probes were incubated in a growth solution prepared based on a protocol described elsewhere [38]. Detailed role of each chemical constituents in the growth solution is extensively discussed by C. J. Murphy et al. [39]. Briefly, 10 μL of $HAuCl_4$ (33 mM) and 6 μL of $AgNO_3$ (20 mM) were added to 964-μL CTAB solution (0.1 M) and mixed gently in a plastic vial (Eppendorf tube). Next, 20 μL of freshly prepared ascorbic acid (0.1 M) was added to this mixture which resulted in a color change from yellow to colorless.

Experimental Setup

The optical setup mainly consists of a halogen light source (HL2000 with a wavelength range 360 to 2400 nm) and a fiber optic spectrometer (USB 4000) with wavelength range between 200 and 1000 nm that were procured from Ocean Optics Inc, USA.

After sputter deposition, one end of the Ni-seeded U-bend fiber was connected to the halogen light source (using SMA 905 connector) and the other end was connected to a fiber optic spectrometer with the help of bare fiber adapters (BFT1, Thorlabs Inc., USA) and compatible SMA connectors as depicted in Fig. 1b. The UV-visible absorption spectra were recorded in real-time using Spectrasuite software.

Sucrose Solutions

Different refractive index (RI) solutions were prepared by adding various amount of sucrose in DI water and their RI (1.333 to 1.348) was verified using a standard bench-top refractometer (J357. Rudolph Research, USA). The probes were dipped into the sucrose solutions of increasing RI values and absorbance spectral response were recorded with DI water as reference.

Chemical and Mechanical Stability Tests

The chemical stability of the plasmonic GOF and POF probe was evaluated by dipping them in 1 M H_2SO_4, 1 M NaOH, H_2O_2, or PBS (1×) solutions for 1 h and monitoring the plasmonic peak absorbance. The mechanical stability test was carried out using a scotch tape (3 M scotch tape 810 magic). First, the probe was connected to a light source and a spectrometer and its U-region was placed on a clean glass slide. Next, the adhesive side of a scotch tape was pressed against the U-region of the AuNSs-probe and pulled off manually, while observing the changes in the plasmonic EWA peak in real-time. This procedure was repeated twice which was indicated as three cycles. For stability studies, a highly stable white LED light source (built in-house) was used.

SERS-Based Sensing

Feasibility of plasmonic POF probes as a SERS substrate was examined. Here, AuNSs-coated POF probes were dipped (for 3 h) in varying concentrations of aqueous Rhodamine B dye solution (Raman label). SERS signals were acquired using a benchtop Raman spectrometer (TEC cooled WP 785L, Wasatch Photonics, USA) in a conventional backscattering configuration. Here, 785-nm laser source was operated at 40 mW power. Integration time was kept at 1 s with average of 5 scans. Raman scattering spectra were acquired using Enlighten software.
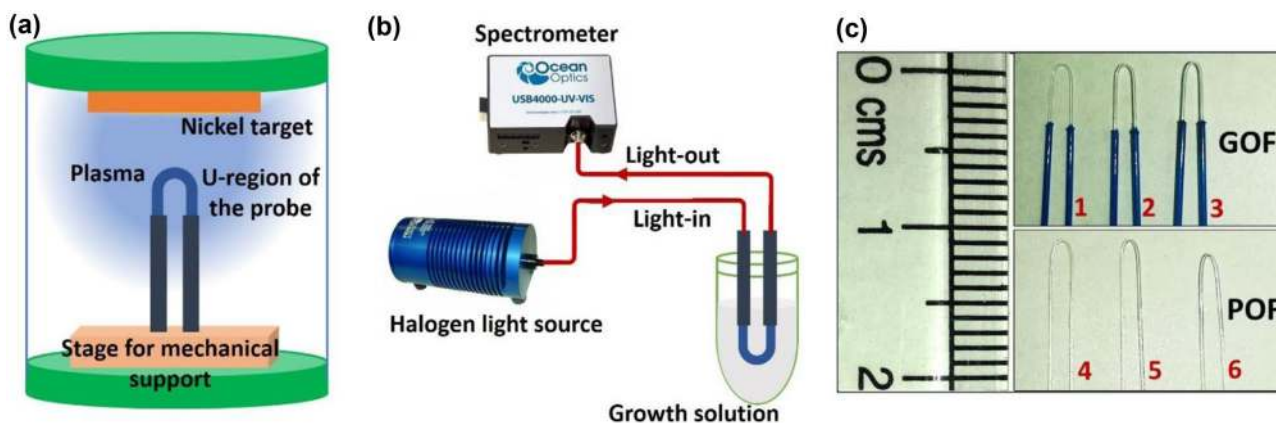
Fig. 1 Experimental setup. (**a**) Schematic presentation of Ni-coating inside a sputtering chamber. (**b**) Illustration of the optical setup for fabricating plasmonic fiber optic probes. (**c**) Actual photographic image of (1,4) bare-(2,5) Ni-sputtered-(3,6) AuNPs grown-GOF and POF probes

Characterization

The plasmon peak in EWA-based UV-visible spectrum was obtained by calculating minimum dA/dλ using Origin software. Roughness measurements were made using atomic force microscope (AFM, NX10 Park system) in a non-contact mode at a scan rate of 0.5 Hz. Scanning electron microscopy (SEM) imaging and the energy dispersive X-ray (EDX) analysis were performed using Hitachi S-4800 attached with an Oxford instrument X-Max 80 mm^2 detector. SEM imaging was carried out with an accelerating voltage of 5.0 kV and working distance of 8.1 mm.

Results and Discussion

Seed Deposition on the U-Bent Probes

Sensitivity of plasmonic U-bent fiber optic probes depends on the effective interaction of metal nanostructures with evanescence field at the core-medium interface [40].

Simulation studies show that maximum light is confined at the outer curvature of the U-region of the probe (Fig. S3, in Supplementary Information) [41]. Therefore, we aim to grow AuNSs by seeding Ni at the outer U-bent region for sensor probe. To achieve this, the probes were held vertically close to the center of the ring target in the sputter-deposition unit. For both GOF and POF probes, Ni was sputter coated on the decladded U-region for a deposition time of 10 s. After sputtering, the EWA spectra of Ni-coated probes were obtained by dipping them in DI water while bare U-bent probe was taken as reference (Fig. 2a). These spectra consistently revealed the presence of an absorbance peak at ~ 390 and 385 nm for Ni-sputtered GOF and POF probes, respectively ($n = 5$). The AFM images obtained from Ni-coated GOF and POF probes (Fig. 2b) sputtered for 10 s substantiate the formation of nano-islands on the probe surface. The RMS roughness (in nm) of the bare and Ni-sputtered fiber surfaces was (5, 9) and (4, 7) for GOF and POF, respectively. This considerable increase in the roughness indicates the formation of Ni seeds of
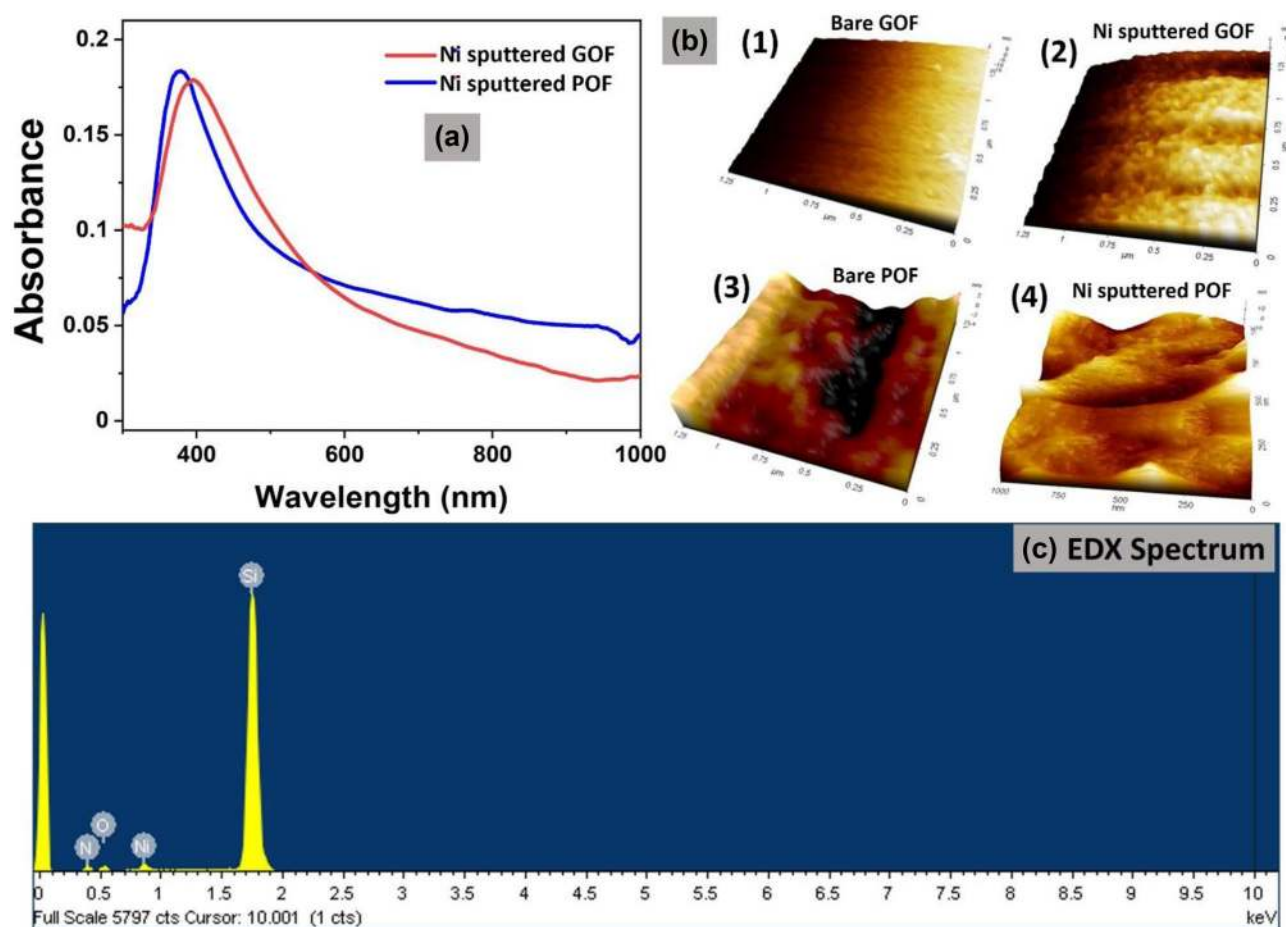
Fig. 2 (a) EWA-based UV-visible spectra recorded from Ni/NiO coated U-bent GOF and POF probe (10 s sputtered) using a fiberoptic spectrometer and broadband halogen light source. (b) AFM images of bare and sputtered GOF and POF probes (near the outer curvature). (c) EDX spectrum of Ni-sputtered silicon wafer with a Si_3N_4 surface showing nickel (2.67 wt%) and oxygen (1.14 wt%) peaks

dimensions around 3 to 5 nm. To investigate the elemental composition, Ni-sputtered silicon wafer (under same experimental conditions) was subjected to EDX analysis. Presence of nickel with oxygen on the sputtered silicon wafers was confirmed using EDX spectra (Fig. 2c). This points a potential formation of Ni/NiO layer on the U-bent probes, which could be attributed to the presence of oxygen ambience due to the low vacuum conditions (3 Pa) as well as oxidized Ni on the target surface (Fig. S4, in Supplementary Information) [42, 43]. The optical absorption spectral characteristics with a peak around 390 nm obtained from the Ni-sputtered U-bent probes is similar to those of freely suspended NiO nanoparticles in the size range of 3 to 5 nm reported elsewhere [44, 45]. Interestingly, the EWA spectra of the probes sputter coated for 50 s were significantly broader over 400 to 1000 nm, with a peak beyond 500 nm wavelength, pointing towards formation of a continuous Ni/NiO film over the probe surface (Fig. S5, in Supplementary Information).

Since the primary goal of the study was to fabricate LSPR-active plasmonic fiber optic probes, the sputtering time was kept low ($t = 10$ s) in order to obtain discrete seed particles. It may be noted that after sputter deposition, the probes were used as-such without any thermal treatment.

Seed-Mediated Growth of Gold Nanostructures

The seed-mediated growth strategy adopted in this study has been well-established to synthesize anisotropic AuNSs using metal seeds such as Fe, Ru, Cd, Cu, Hg, In, Au, or Sb in colloidal solutions [46]. In our case, AuNSs were grown on Ni/NiO-seeded GOF and POF probes by dipping them into an aqueous growth solution containing CTAB, HAuCl$_4$, AgNO$_3$, and ascorbic acid. The formation of the AuNSs on the U-bent probes was monitored in real-time and the EWA spectra were recorded at regular intervals during the growth process. Figure 3 shows a very interesting phenomenon, where, as soon as the Ni-sputtered GOF probe was dipped in the growth solution, the optical absorption characteristics of Ni/NiO seeds were found to rapidly diminish from 0.16 to almost 0.015 units within the first 30 s with a blue-shift in the peak from 390 to ~ 360 nm.

Soon after, a plasmonic characteristic peak at 550 nm was observed at 60 s indicating the deposition of gold over the probe surface. Within 11 min, a remarkable 2-orders of increase in the plasmonic absorbance with a red-shift in its plasmon peak (50 nm) was observed (Fig. 4a), indicating the growth phase with a continued deposition of gold over the nucleation sites and leading to the formation of AuNSs. When the absorbance response reached a value of 2.0 units, the growth of AuNSs were arrested by removing GOF probe from growth solution and rinsing the probe surface with DI water. Newly formed AuNSs contributed to a plasmon

peak at 600 nm for GOF probe. SEM images confirmed the presence of discrete AuNSs formation with irregular shape on silica surface (Fig. 4b, c). The packing density of AuNSs on the outer region was much higher compared with the inner region on the U-bend portion of GOF probes (Fig. S6, in Supplementary Information). This result confirms that higher AuNSs packing on the outer curvature could lead to effective interaction of nanostructures with evanescent field. On the other hand, AuNSs were formed on Ni-sputtered POF probe and exhibited a plasmonic peak at 570 nm (Fig. 4d). The shape and size of AuNSs on PMMA surface of POF probes were also found to be irregular with polydispersity (Fig. 4e, f). In both GOF and POF probes, it was interesting to observe the colorless growth solution turning into pink color during AuNSs formation. In control experiments, no AuNSs were grown on the probes nor the growth solution turned pink in the case of bare U-bent probes without Ni sputtered seeds.

To the best of our knowledge, this study is the first report that demonstrates the use of Ni/NiO for the seed-mediated AuNSs synthesis on an optical fiber sensor probe. While an established scientific explanation for the growth of AuNSs over Ni/NiO is limited in the literature, we anticipate the following plausible explanation based on the experimental evidence. We anticipate AuNSs growth over the Ni/NiO seeds as a consequence of reducing agent-assisted galvanic replacement (ascorbic acid in growth solution) of Ni with Au [47, 48]. During AuNSs formation, Ni ions would partially dissolve into the growth solution followed by metallic Au deposition on the seed layer [49, 50]. The dissolved Ni ions in the growth solution also act as nucleation sites and initiate the
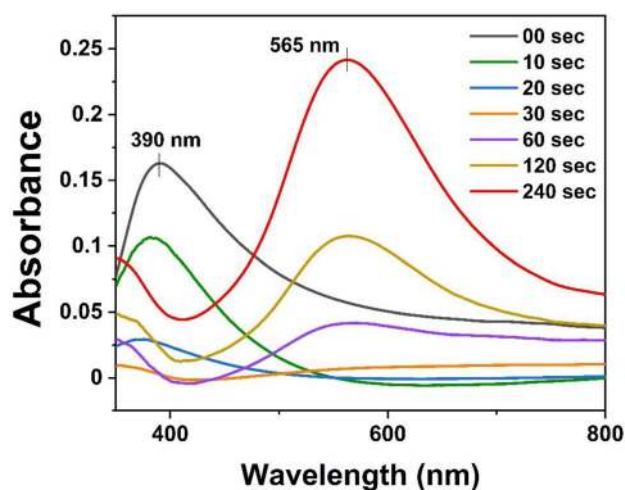
Fig. 3 EWA spectra recorded from GOF U-bent probe during the AuNSs growth phase showing sacrificial deposition of Au on Ni/NiO seeds by reducing agent-assisted galvanic replacement
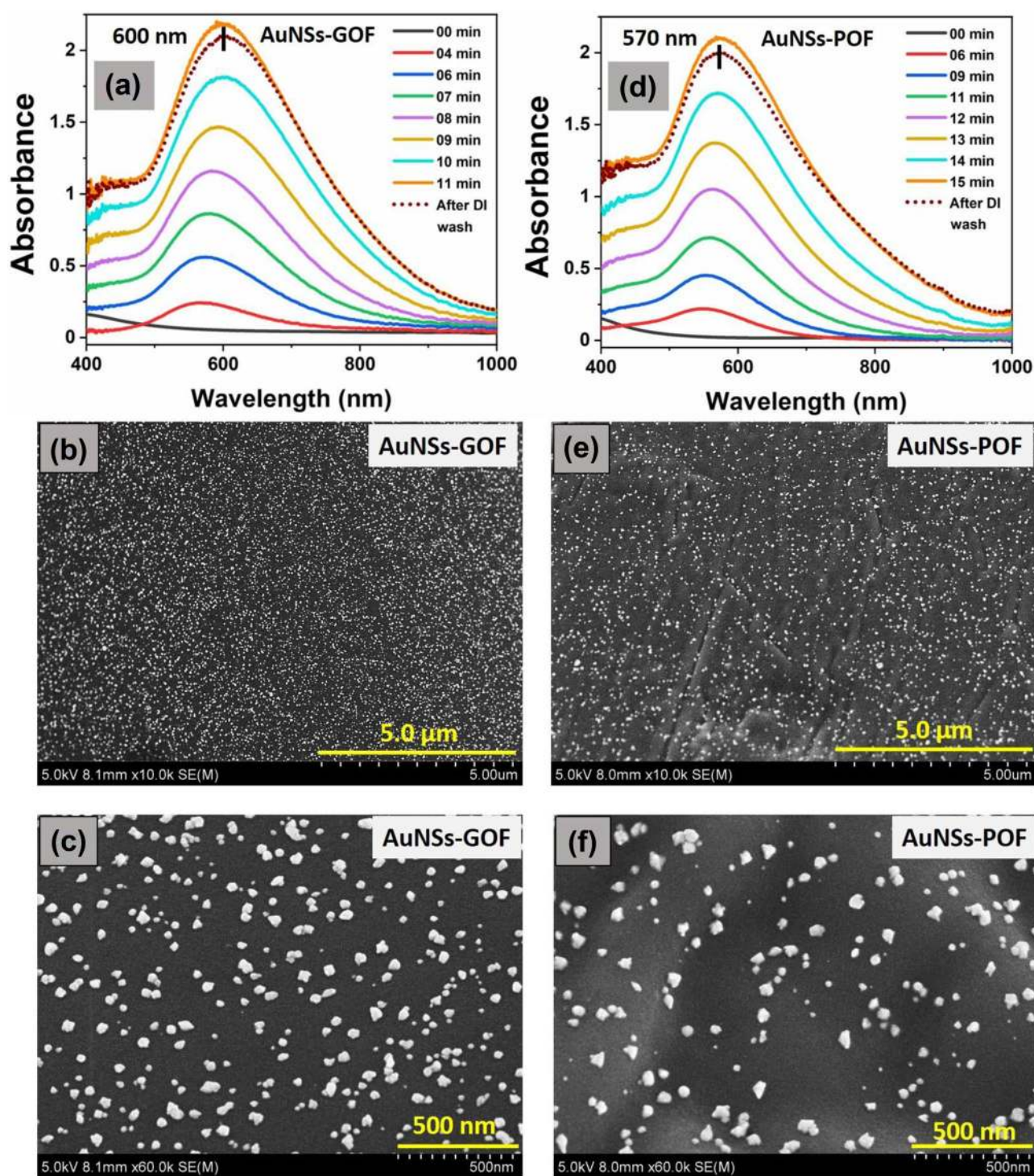
Fig. 4 Formation of AuNSs on Ni/NiO seeded U-bent GOF and POF probes. Monitoring the growth kinetics of AuNSs by recording EWA spectra (**a, d**). SEM images of AuNSs (**b, c** and **e, f**) formed on GOF and POF probe surface, respectively

growth of gold nanoparticles, suggesting it as a potential reason for the pink coloration of growth solution. In absence of Ni/NiO seeds, no AuNSs were formed on the bare fiber probes when immersed in growth solution. The results indicate that Ni seeds are essential for AuNSs

synthesis. Thus, it may be concluded that the Ni/NiO seeds act as a sacrificial template that serve as nucleation, growth, and anchoring sites for AuNSs. This in situ seed-mediated growth technique led to the synthesis of discrete nanostructures on the fiber probes.

Refractive Index Sensitivity

Refractive index (RI) sensitivity is an important characteristic to evaluate the sensing performance of a LSPR sensor. Monitoring the absorbance based intensity modulation instead of wavelength shifts can be very useful for designing compact LSPR-based fiber optic sensors with simple photodetectors (eliminating optical components such as diffraction gratings and mirrors) [51]. In the EWA-based plasmonic U-bent fiber optic probes, an RI change in the vicinity of AuNSs on the probe surface leads to a change in the absorbance peak. For plasmonic POF and GOF probes, RI sensitivity is defined as the ratio of the change in absorbance value per refractive index unit ($\Delta A/\Delta RIU$). In our experiments, bare, Ni/NiO-seeded, and AuNSs-coated GOF or POF probes were dipped in varying RI solutions (1.333 to 1.351) and

their respective LSPR spectra were recorded as shown in Fig. 5 a and 5c, respectively. The EWA spectral characteristics revealed a peak plasmonic absorbance at 600 and 570 nm for GOF and POF probes, respectively. The peak absorbance values were recorded and plotted against RI to calculate RI sensitivity ($n=3$). For bare, Ni/NiO-seeded and AuNSs-coated GOF probes, the RI sensitivity values obtained after fitting a linear regression curve were 4.35, 8.64, and 27.66 $\Delta A/\Delta RIU$, respectively (Fig. 5b). On the other hand, the RI sensitivity of 3.48, 7.13, and 25.65 $\Delta A/\Delta RIU$ were obtained for bare, Ni/NiO-seeded, and AuNSs-coated POF, respectively (Fig. 5d). The sensor showed excellent linearity with $R^2=0.999$ for both GOF and POF probes. The RI sensitivities of the bare, Ni/NiO-seeded, and plasmonic GOF probes were slightly higher (8 to 20%) than that of POF. The difference is more pronounced in case of bare probes (20% higher), which
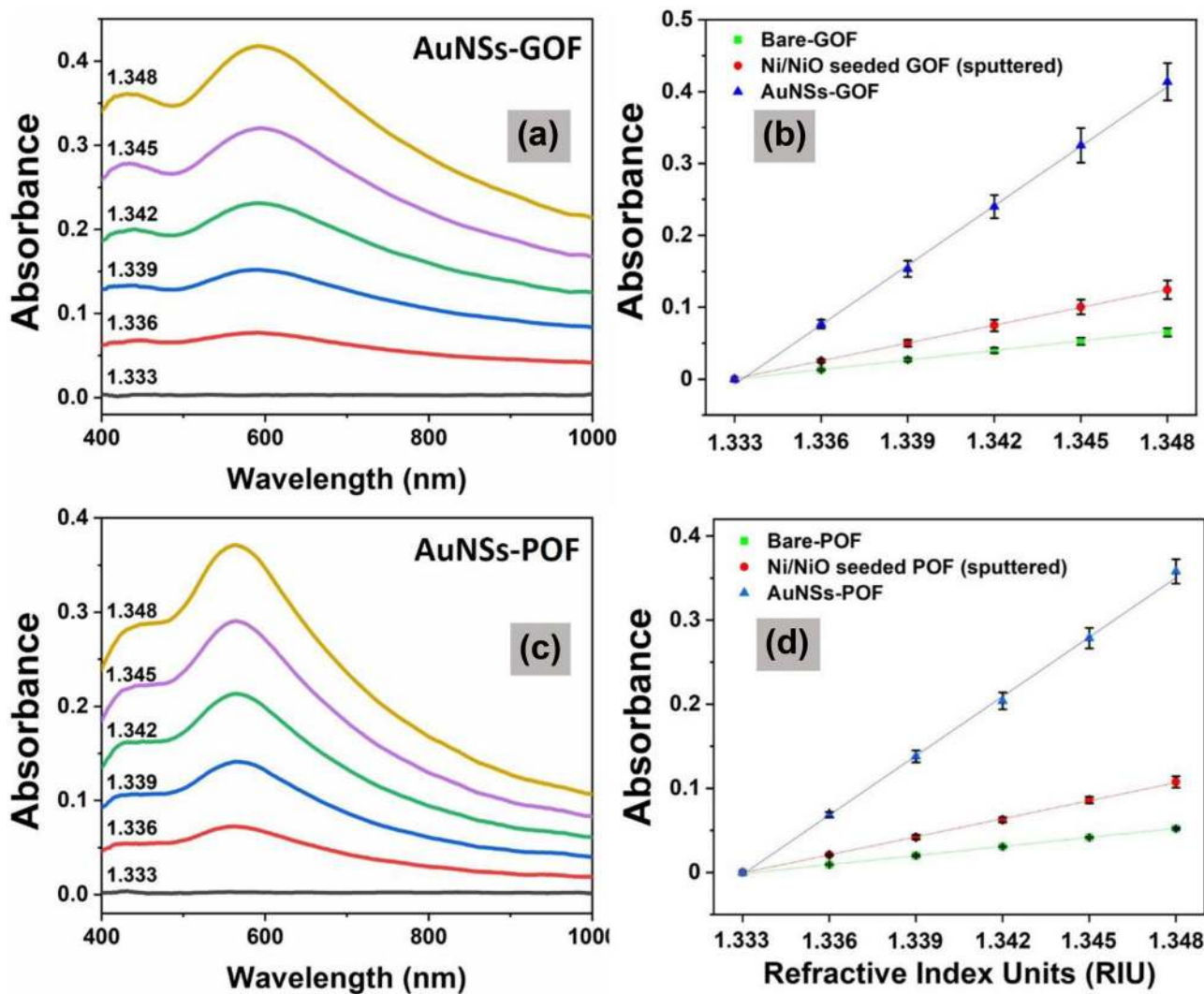

Fig. 5 LSPR-based RI sensitivity measurements. EWA spectral response and RI sensitivity of plasmonic GOF (**a**, **b**) and POF (**c**, **d**) probes in the presence of solution with RI value from 1.333 to 1.348 RIU

could be due to a better EWA sensitivity caused by the smaller (20%) core diameter of the GOF. Recently, Zewei Luo et al. have fabricated ultrasensitive plasmonic U-shaped fiber optic sensor with a LSPR-based RI sensitivity of ~24.66 ΔA/ΔRIU [52]. In that report, they were able to sense cancer cells in a label-free format with a detection limit of 30 cells/mL. From our results, plasmonic U-bent probes achieved a RI sensitivity of ~26 ΔA/ΔRIU indicating that these probes can be a valuable tool for label-free biomolecular detection.

Chemical and Mechanical Stability

It is important to test chemical and mechanical stability of the plasmonic probes, as these fiber optic sensors are deployable in wide range of sensing applications involving harsh environment. For chemical stability testing, individual plasmonic GOF and POF probes were dipped either in H_2SO_4 (1 M), NaOH (1 M), H_2O_2 (30%), or PBS (1 ×) solutions for 1 h. The time-dependent changes in the EWA peak at 600 nm and 570 nm were monitored for GOF and POF probes, respectively (Fig. 6a, b). Plasmonic GOF probe showed 12.5% and 3% absorbance decrement in NaOH and H_2O_2 solution, respectively, indicating a desorption of AuNSs from the probe surface. In comparison, the plasmonic POF probes were highly stable in all solvents except in NaOH (2% absorbance decrement). We attribute the anchoring of Ni/NiO seeds with the fiber core material (PMMA) of the POF due to softening of the POF during the sputter process offering a stronger adhesion of the AuNSs to the probe surface [20].

Mechanical stability of the synthesized AuNSs on fiber probe surface was evaluated by peel test using a scotch tape

(adhesive strength of 2.5 N/cm) as shown in Fig. 7a. The changes in absorbance were monitored in real-time using a fiber optic spectrometer (Fig. 7b). After each cycle, the peak absorbance was found to decrease (Fig. 7c). At the end of 3rd adhesive cycle, there was about ~23% and ~27% drop in initial absorbance for plasmonic GOF and POF, respectively. This peel test confirms that the AuNSs strongly adhere to silica and PMMA surface.

Plasmonic POF Probes as SERS-Active Substrates

PMMA substrates are promising candidate for SERS applications as they are stable, flexible, transparent, and inexpensive [53, 54]. As AuNSs-coated POF probes exhibited excellent chemical stability, they were chosen as SERS substrates to detect rhodamine B (RhB) dye at various concentrations (Fig. 8a, b). In a backscattered configuration, Raman scattering spectra were collected from at least three different regions on each plasmonic POF probe ($n = 3$) subjected to a given RhB concentration and their average was plotted as shown in Fig. 8c. The most prominent bands in the 1000 to 1600 cm^{-1} region of the spectrum match well with the spectral characteristics of RhB dye. The SERS spectral characteristic peaks at 1278, 1357, and 1508 cm^{-1} indicate the vibrational modes of the aromatic C–H bending, aromatic C–C bending, and aromatic C–H bending, respectively [55]. The results showed that the SERS intensity increased with RhB concentrations with a detection limit of 10^{-7} RhB. Recently, Yang Ran et al. were able to detect 10^{-7} to 10^{-8} M RhB using fiber-optrode SERS probes coated with plasmonic silver-coated gold nanostars [56]. These results indicate that plasmonic POF can be a potential SERS substrate for detecting chemical analytes.

Fig. 6 Chemical stability of plasmonic GOF (**a**) and POF (**b**) probes evaluated for 1 h in the presence of harsh chemical environment
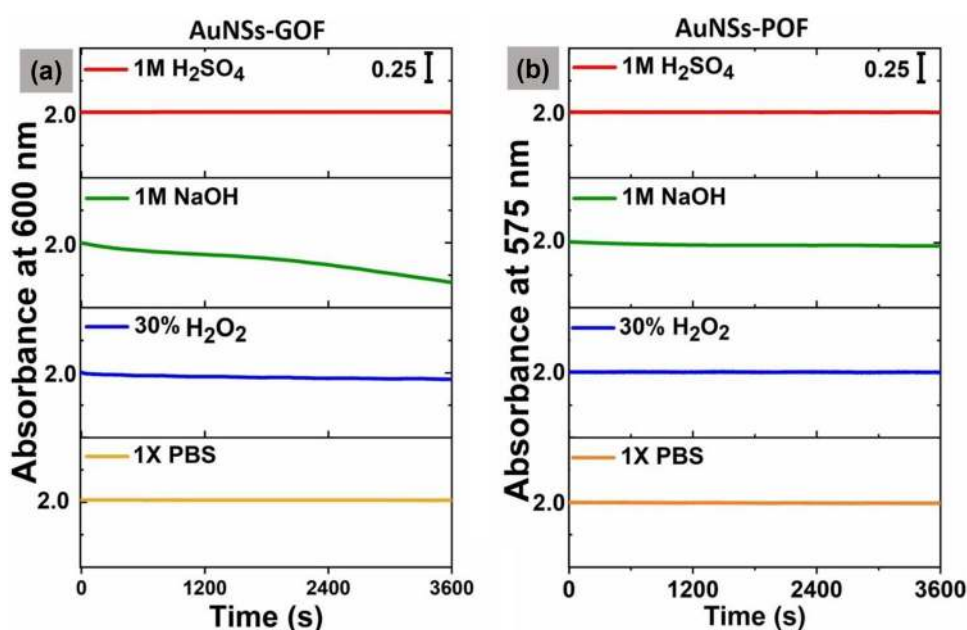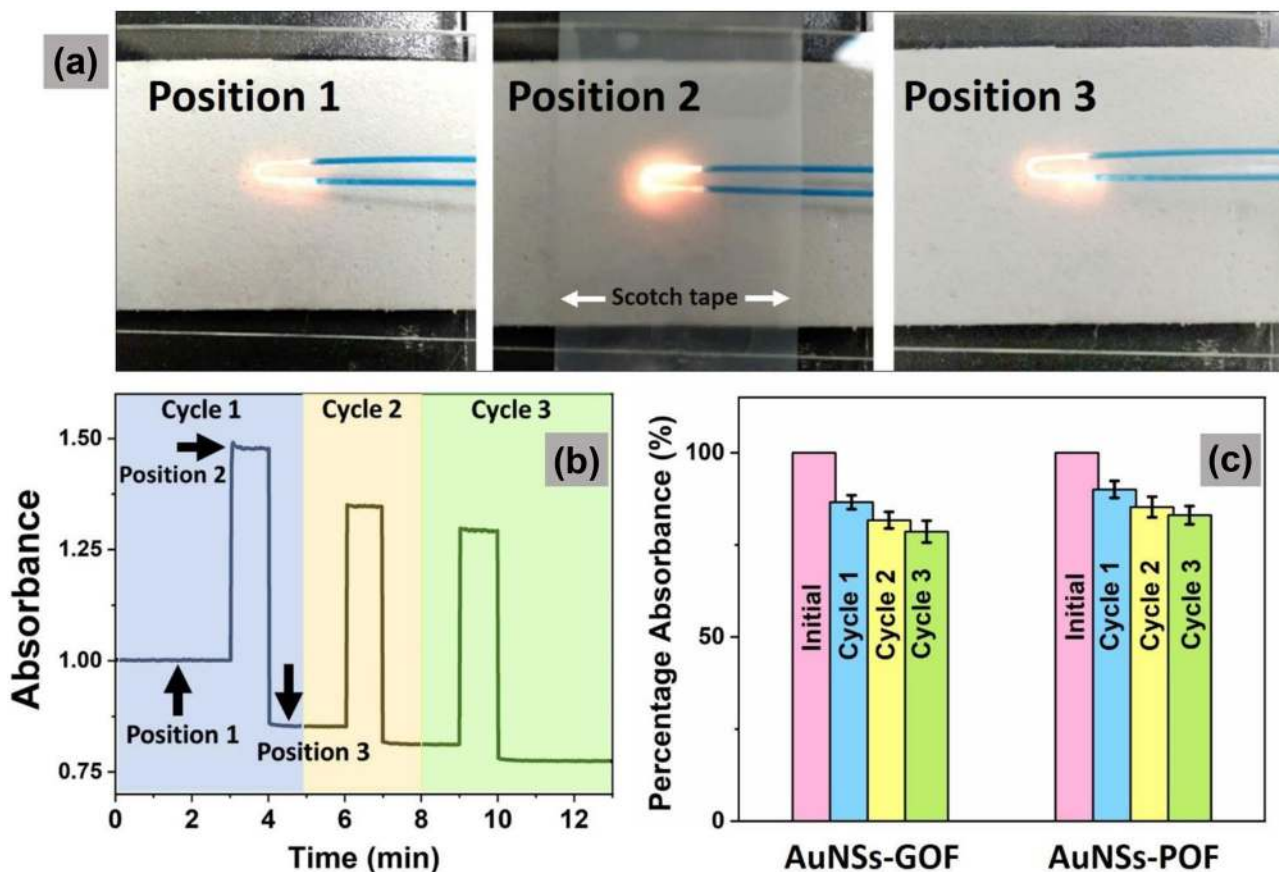
Fig. 7 Mechanical stability of the plasmonic probes. (**a**) Experimental procedure for peel test using an adhesive tape. (**b**) Real-time monitoring of absorbance change during peel test. (**c**) Loss in absorbance (at 600 nm and 570 nm at their plasmonic peaks) after each cycle for plasmonic GOF and POF, respectively
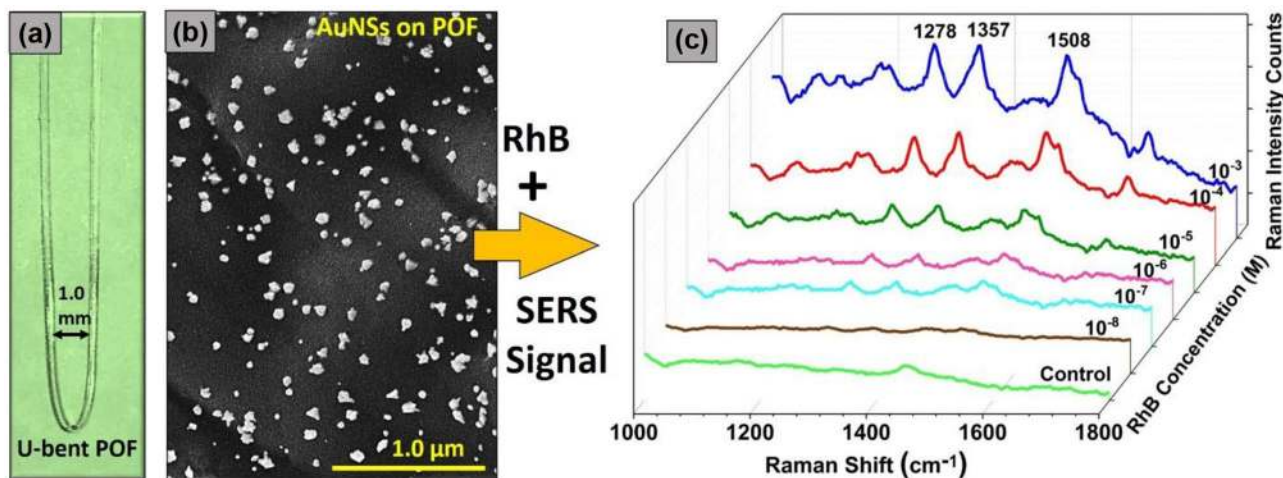

Fig. 8 Plasmonic POF probe for SERS-based chemical sensing. (**a**) Photographic image of plasmonic U-bent POF and (**b**) SEM image of AuNSs. (**c**) SERS spectra of RhB (at various concentrations) adhered to AuNSs on the U-bent POF

Conclusions

This study demonstrates a simpler and faster technique to fabricate plasmonic fiber optic sensors probes by combining the advantages of reproducible physical process of sputtering for Ni/NiO seeds and controlled chemical process for AuNSs growth. This technique is shown to be suitable for both U-bent GOF and POF probes. In addition, this technique allows the seeds to be confined to the outer curvature of the U-bent probes thus leading to high sensitivity due to an efficient excitation and measurement of the LSPR characteristics of the AuNSs. Excellent chemical stability, good mechanical stability and reliable LSPR spectral response are the unique features of this technique in comparison with the conventional chemisorption based techniques that are plagued by surface fouling. This seed-mediated growth technique eliminates the need of thermal treatment processes which usually improve AuNSs adhesion. In addition, Ni/NiO seeds do not impede the spectral characteristics and sensitivity of the sensors. In summary, the sputter seed-mediated growth of AuNSs established in this study is highly promising for the large-scale manufacture of the fiber optic LSPR sensors.

Data Availability The datasets generated during and/or analyzed during the current study are available from the corresponding author on reasonable request.

Declarations

Conflict of Interest The authors declare that they have no conflict of interest.

References

1. Wang X, Wolfbeis OS (2020) Fiber-optic chemical sensors and biosensors (2015–2019). Anal Chem 92:397–430. https://doi.org/10.1021/acs.analchem.9b04708
2. Zhao Y, Tongjie, Xia F, Peng Y R (2019) Current status of optical fiber biosensor based on surface plasmon resonance. Biosens Bioelectron 142:111505. https://doi.org/10.1016/j.bios.2019.111505
3. Esfahani Monfared Y (2020) Overview of recent advances in the design of plasmonic fiber-optic biosensors. Biosensors 10:77. https://doi.org/10.3390/bios10070077
4. Qu JH, Dillen A, Saeys W et al (2020) Advancements in SPR biosensing technology: an overview of recent trends in smart layers design, multiplexing concepts, continuous monitoring and in vivo sensing. Anal Chim Acta 1104:10–27. https://doi.org/10.1016/j.aca.2019.12.067
5. Sharma AK, Pandey AK, Kaur B (2018) A review of advancements (2007–2017) in plasmonics-based optical fiber sensors. Opt Fiber Technol 43:20–34. https://doi.org/10.1016/j.yofte.2018.03.008
6. Estevez MC, Otte MA, Sepulveda B, Lechuga LM (2014) Trends and challenges of refractometric nanoplasmonic biosensors: a review. Anal Chim Acta 806:55–73. https://doi.org/10.1016/j.aca.2013.10.048
7. Caucheteur C, Guo T, Albert J (2015) Review of plasmonic fiber optic biochemical sensors: improving the limit of detection. Anal Bioanal Chem 407:3883–3897. https://doi.org/10.1007/s00216-014-8411-6
8. Rivero PJ, Goicoechea J, Arregui FJ (2017) Localized surface plasmon resonance for optical fiber-sensing applications. In: Nanoplasmonics - Fundam Appl InTech. https://doi.org/10.5772/67544
9. Bilro L, Alberto N, Pinto JL, Nogueira R (2012) Optical sensors based on plastic fibers. Sensors 12:12184–12207. https://doi.org/10.3390/s120912184
10. Liang G, Luo Z, Liu K et al (2016) Fiber optic surface plasmon resonance-based biosensor technique: fabrication, advancement, and application. Crit Rev Anal Chem 46:213–223. https://doi.org/10.1080/10408347.2015.1045119
11. Miliutina E, Guselnikova O, Chufistova S et al (2019) Fast and all-optical hydrogen sensor based on gold-coated optical fiber functionalized with metal-organic framework layer. ACS Sensors 4:3133–3140. https://doi.org/10.1021/acssensors.9b01074
12. Klantsataya E, Jia P, Ebendorff-Heidepriem H et al (2016) Plasmonic fiber optic refractometric sensors: From conventional architectures to recent design trends. Sensors 17:12. https://doi.org/10.3390/s17010012
13. Qian Y, Zhao Y, Wulu Q, Yang Y (2018) Review of salinity measurement technology based on optical fiber sensor. Sensors Actuators B Chem 260:86–105. https://doi.org/10.1016/j.snb.2017.12.077
14. Velázquez-González JS, Monzón-Hernández D, Moreno-Hernández D et al (2017) Simultaneous measurement of refractive index and temperature using a SPR-based fiber optic sensor. Sensors Actuators B Chem 242:912–920. https://doi.org/10.1016/j.snb.2016.09.164

15. Wei Y, Wu P, Zhang Y et al (2019) A new application of optical fiber surface plasmon resonance for micro-displacement measurement. Sensors Actuators A Phys 285:216–223. https://doi.org/10.1016/j.sna.2018.11.007

16. Wang J, Geng Y, Shen Y et al (2019) SERS-active fiber tip for intracellular and extracellular pH sensing in living single cells. Sensors Actuators B Chem 290:527–534. https://doi.org/10.1016/j.snb.2019.03.149

17. Zhang JZ, Noguez C (2008) Plasmonic optical properties and applications of metal nanostructures. Plasmonics 3:127–150. https://doi.org/10.1007/s11468-008-9066-y

18. Zhang Y, Wang G, Yang L et al (2018) Recent advances in gold nanostructures based biosensing and bioimaging. Coord Chem Rev 370:1–21. https://doi.org/10.1016/j.ccr.2018.05.005

19. Masson J-F (2020) Portable and field-deployed surface plasmon resonance and plasmonic sensors. Analyst 145:3776–3800. https://doi.org/10.1039/D0AN00316F

20. Christopher C, Subrahmanyam A, Sai VVR (2018) Gold sputtered U-bent plastic optical fiber probes as SPR- and LSPR-based compact plasmonic sensors. Plasmonics 13:493–502. https://doi.org/10.1007/s11468-017-0535-z

21. Antohe I, Schouteden K, Goos P et al (2016) Thermal annealing of gold coated fiber optic surfaces for improved plasmonic biosensing. Sensors Actuators B Chem 229:678–685. https://doi.org/10.1016/j.snb.2016.02.034

22. Cheng S, Chau L (2003) Colloidal gold-modified optical fiber for chemical. Anal Chem 75:16–21. https://doi.org/10.1021/ac020310v

23. Aouani H, Wenger J, Gérard D et al (2009) Crucial role of the adhesion layer on the plasmonic fluorescence enhancement. ACS Nano 3:2043–2048. https://doi.org/10.1021/nn900460t

24. Hoey ML, Carlson JB, Osgood RM et al (2010) rf plasma oxidation of Ni thin films sputter deposited to generate thin nickel oxide layers. Appl Phys Lett 97:153104. https://doi.org/10.1063/1.3499661

25. Sexton BA, Feltis BN, Davis TJ (2008) Characterisation of gold surface plasmon resonance sensor substrates. Sensors Actuators A Phys 141:471–475. https://doi.org/10.1016/j.sna.2007.10.020

26. Zhu M, Lerum MZ, Chen W (2012) How to prepare reproducible, homogeneous, and hydrolytically stable aminosilane-derived layers on silica. Langmuir 28:416–423. https://doi.org/10.1021/la203638g

27. Scarpettini AF, Bragas AV (2010) Coverage and aggregation of gold nanoparticles on silanized glasses. Langmuir 26:15948–15953. https://doi.org/10.1021/la102937b

28. Manoharan H, KC D, Sai VVR, (2020) controlled in situ seed-mediated growth of gold and silver nanoparticles on an optical fiber platform for plasmonic sensing applications. Plasmonics 15:51–60. https://doi.org/10.1007/s11468-019-01008-6

29. Gong Y, Zhang S, Gao H et al (2020) Recent advances and comprehensive insights of nickel oxide in emerging optoelectronic devices. Sustainable Energy Fuels 17–33. https://doi.org/10.1039/D0SE00621A

30. Kate RS, Khalate SA, Deokate RJ (2018) Overview of nanostructured metal oxides and pure nickel oxide (NiO) electrodes for supercapacitors: a review. J Alloys Compd 734:89–111. https://doi.org/10.1016/j.jallcom.2017.10.262

31. Hajakbari F (2020) Characterization of nanocrystalline nickel oxide thin films prepared at different thermal oxidation temperatures. J Nanostructure Chem 10:97–103. https://doi.org/10.1007/s40097-020-00332-2

32. Aydin E, Troughton J, De Bastiani M et al (2018) Room-temperature-sputtered nanocrystalline nickel oxide as hole transport layer for p-i-n perovskite solar cells. ACS Appl Energy Mater 1:6227–6233. https://doi.org/10.1021/acsaem.8b01263

33. Yang F, Zhou X, Plymale NT et al (2020) Evaluation of sputtered nickel oxide, cobalt oxide and nickel–cobalt oxide on n-type silicon photoanodes for solar-driven O 2 (g) evolution from water. J Mater Chem A 8:13955–13963. https://doi.org/10.1039/D0TA03725G

34. Turgut E, Çoban Ö, Sarıtaş S et al (2018) Oxygen partial pressure effects on the RF sputtered p-type NiO hydrogen gas sensors. Appl Surf Sci 435:880–885. https://doi.org/10.1016/j.apsusc.2017.11.133

35. Oh MH, Yu T, Yu S-H et al (2013) galvanic replacement reactions in metal oxide nanocrystals. Science (80-) 340:964 LP – 968. https://doi.org/10.1126/science.1234751

36. Sai VVR, Kundu T, Mukherji S (2009) Novel U-bent fiber optic probe for localized surface plasmon resonance based biosensor. Biosens Bioelectron 24:2804–2809. https://doi.org/10.1016/j.bios.2009.02.007

37. Gowri A, Sai VVR (2016) Development of LSPR based U-bent plastic optical fiber sensors. Sensors Actuators B Chem 230:536–543. https://doi.org/10.1016/j.snb.2016.02.074

38. Jana NR, Gearheart L, Murphy CJ (2001) Wet chemical synthesis of high aspect ratio cylindrical gold nanorods. J Phys Chem B 105:4065–4067. https://doi.org/10.1021/jp0107964

39. Murphy CJ, Sau TK, Gole AM et al (2005) Anisotropic metal nanoparticles: synthesis, assembly, and optical applications. J Phys Chem B 109:13857–13870. https://doi.org/10.1021/jp0516846

40. Gupta BD, Verma RK (2009) Surface plasmon resonance-based fiber optic sensors: Principle, probe designs, and some applications. J Sensors. 2009:1–12. https://doi.org/10.1155/2009/979761

41. Danny CG, Danny Raj M, Sai VVR (2020) Investigating the refractive index sensitivity of u-bent fiber optic sensors using ray optics. J Light Technol 38:1580–1588. https://doi.org/10.1109/JLT.2019.2958044

42. Riedl H, Koller CM, Munnik F et al (2016) Influence of oxygen impurities on growth morphology, structure and mechanical properties of Ti-Al-N thin films. Thin Solid Films 603:39–49. https://doi.org/10.1016/j.tsf.2016.01.039

43. Payne BP, Biesinger MC, McIntyre NS (2012) Use of oxygen/nickel ratios in the XPS characterisation of oxide phases on nickel metal and nickel alloy surfaces. J Electron Spectros Relat Phenomena 185:159–166. https://doi.org/10.1016/j.elspec.2012.06.008

44. Fominykh K, Feckl JM, Sicklinger J et al (2014) Ultrasmall dispersible crystalline nickel oxide nanoparticles as high-performance catalysts for electrochemical water splitting. Adv Funct Mater 24:3123–3129. https://doi.org/10.1002/adfm.201303600

45. Nama Manjunatha K, Paul S (2015) Investigation of optical properties of nickel oxide thin films deposited on different substrates. Appl Surf Sci 352:10–15. https://doi.org/10.1016/j.apsusc.2015.03.092

46. Samal AK, Sreeprasad TS, Pradeep T (2010) Investigation of the role of NaBH4 in the chemical synthesis of gold nanorods. J Nanoparticle Res 12:1777–1786. https://doi.org/10.1007/s11051-009-9733-8

47. Kang S, Kang K, Huh H et al (2017) Reducing agent-assisted excessive galvanic replacement mediated seed-mediated synthesis of porous gold nanoplates and highly efficient gene-thermo cancer therapy. ACS Appl Mater Interfaces 9:35268–35278. https://doi.org/10.1021/acsami.7b13028

48. R. Daniel J, McCarthy LA, Ringe E, Boudreau D, (2019) Enhanced control of plasmonic properties of silver-gold hollow nanoparticles via a reduction-assisted galvanic replacement approach. RSC Adv 9:389–396. https://doi.org/10.1039/C8RA09364D

49. Huang J, Han X, Wang D et al (2013) Facile synthesis of dendritic gold nanostructures with hyperbranched architectures and their electrocatalytic activity toward ethanol oxidation. ACS Appl Mater Interfaces 5:9148–9154. https://doi.org/10.1021/am402546p

50. Gilroy KD, Farzinpour P, Sundar A et al (2014) Sacrificial templates for galvanic replacement reactions: design criteria for the synthesis of pure pt nanoshells with a smooth surface morphology. Chem Mater 26:3340–3347. https://doi.org/10.1021/cm501418d

51. Cetin AE, Coskun AF, Galarreta BC et al (2014) Handheld high-throughput plasmonic biosensor using computational on-chip imaging. Light Sci Appl 3:e122–e122. https://doi.org/10.1038/lsa.2014.3

52. Luo Z, Wang Y, Xu Y et al (2019) Ultrasensitive U-shaped fiber optic LSPR cytosensing for label-free and in situ evaluation of cell surface N-glycan expression. Sensors Actuators B Chem 284:582–588. https://doi.org/10.1016/j.snb.2019.01.015

53. Bin ZL, Yin J, Zheng YM et al (2014) Self-assembly of Au nanoparticles on PMMA template as flexible, transparent, and highly active SERS substrates. Anal Chem 86:6262–6267. https://doi.org/10.1021/ac404224f

54. Qiu H, Wang M, Jiang S et al (2017) Reliable molecular trace-detection based on flexible SERS substrate of graphene/Ag-nanoflowers/PMMA. Sensors Actuators B Chem 249:439–450. https://doi.org/10.1016/j.snb.2017.04.118

55. Fang C, Agarwal A, Buddharaju KD et al (2008) DNA detection using nanostructured SERS substrates with Rhodamine B as Raman label. Biosens Bioelectron 24:216–221. https://doi.org/10.1016/j.bios.2008.03.032

56. Ran Y, Strobbia P, Cupil-Garcia V, Vo-Dinh T (2019) Fiber-optrode SERS probes using plasmonic silver-coated gold nanostars. Sensors Actuators B Chem 287:95–101. https://doi.org/10.1016/j.snb.2019.01.167

Publisher's Note Springer Nature remains neutral with regard to jurisdictional claims in published maps and institutional affiliations.